Electronic Supplementary Material (ESI) for Journal of Materials Chemistry C.


# Supporting Information

## Room-temperature Infrared Photothermoelectric Detector Design Based on CNT/PEDOT:PSS Composite

Jiaqi Wang[1], Zhemiao Xie[1], Jiayu Alexander Liu[1], John T.W. Yeow[1]

1. Advanced Micro-/Nano- Devices Lab, Department of Systems Design Engineering, University of Waterloo, 200 University Ave West, Waterloo, Ontario N2L 3G1, Canada

Corresponding Author: John T.W. Yeow

E-mail: jyeow@uwaterloo.ca

Phone: +1-519-888-4567, ext32152

Corresponding author. Tel: 519-888-4567 x32152. Email: jyeow@uwaterloo.ca (John T.W. Yeow)

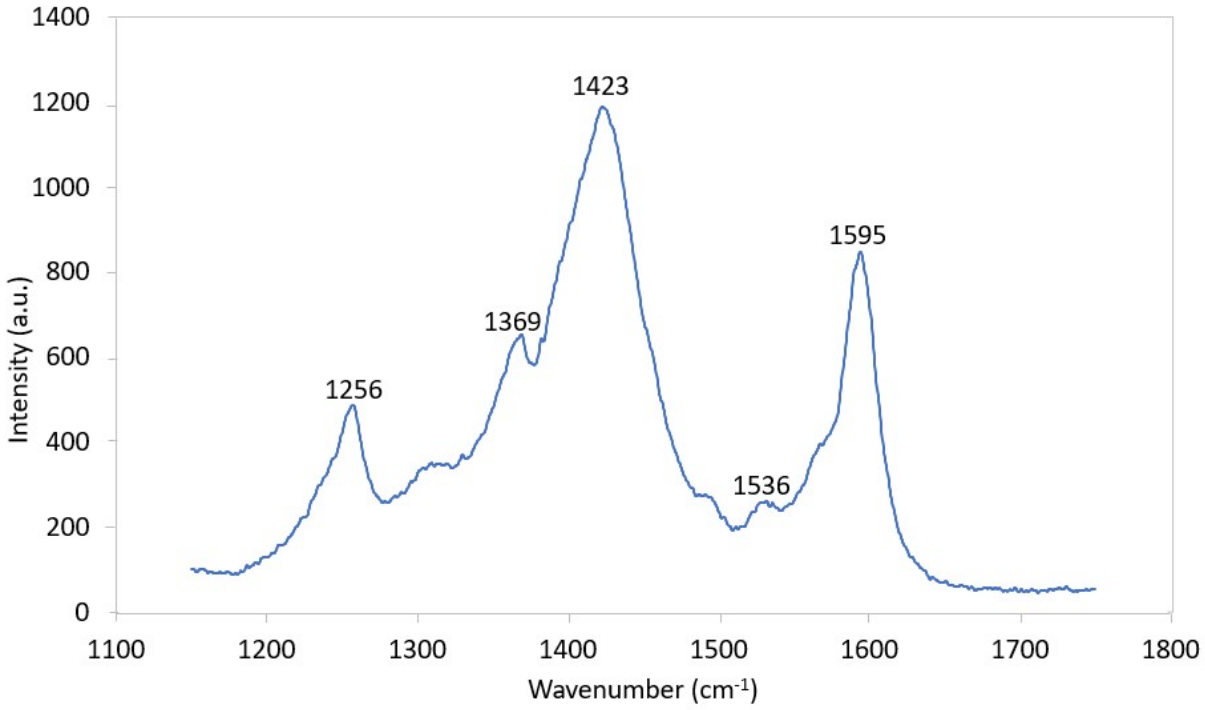


**Figure S1.** Raman spectrum of the 20 wt% SWCNT/PEDOT:PSS composite.

The Raman spectrum of 20 wt% SWCNT/PEDOT:PSS composite is shown in **Figure S2**. The characteristic peak at 1595 $cm^{-1}$ in the composite shows a graphite $E_{2g}$ (G) mode. Other bands are shown on the spectrum that can be explained as $C_\alpha$=$C_\beta$ asymmetrical stretching (1536 $cm^{-1}$), $C_\alpha$=$C_\beta$ symmetric stretching deformation in the aromatic thiophene ring (1423 $cm^{-1}$), $C_\beta$-$C_\beta$ intra-thiophene ring (1369 $cm^{-1}$), $C_\alpha$-$C_\alpha$ inter-ring stretching (1256 $cm^{-1}$) [1–3]. Compared with the Raman spectra of pristine PEDOT:PSS membrane measured in Ref. [4], the $C_\alpha$=$C_\beta$ symmetric stretching shifts from 1433 $cm^{-1}$ to 1423 $cm^{-1}$ in 20 wt% CNT loadings' composite. The shift demonstrates that the π-π interaction is improved between SWCNT and PEDOT chains.

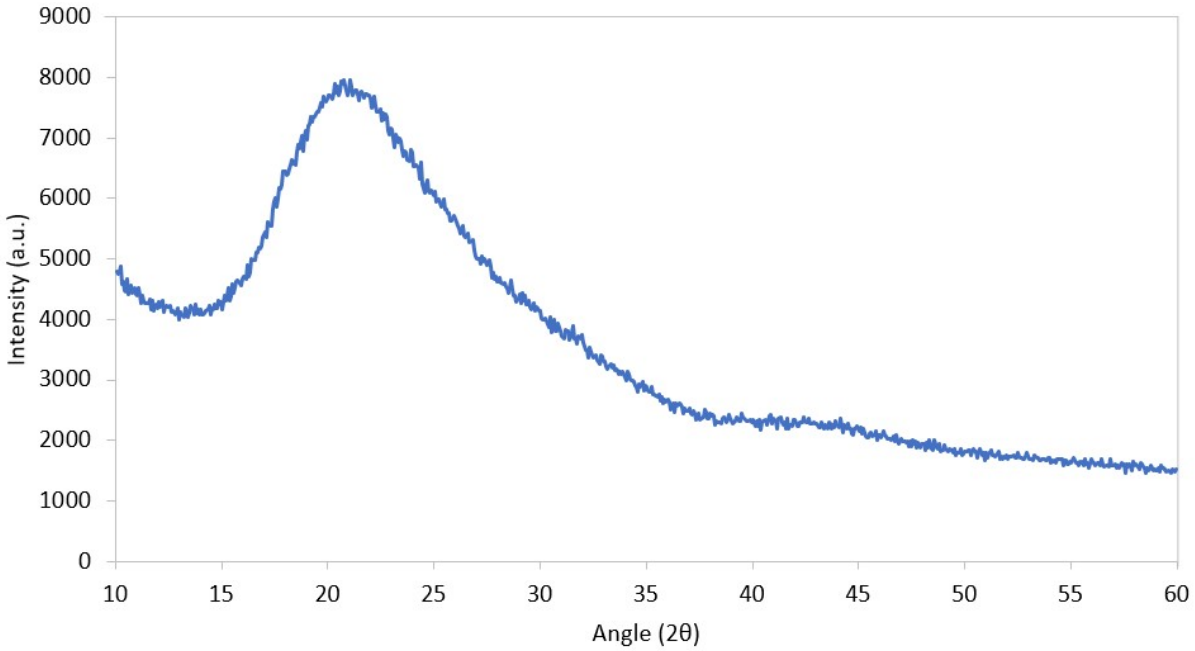


**Figure S2.** Grazing Incidence X-ray Diffraction (GIXRD) of the 20 wt% SWCNT/PEDOT:PSS composite.

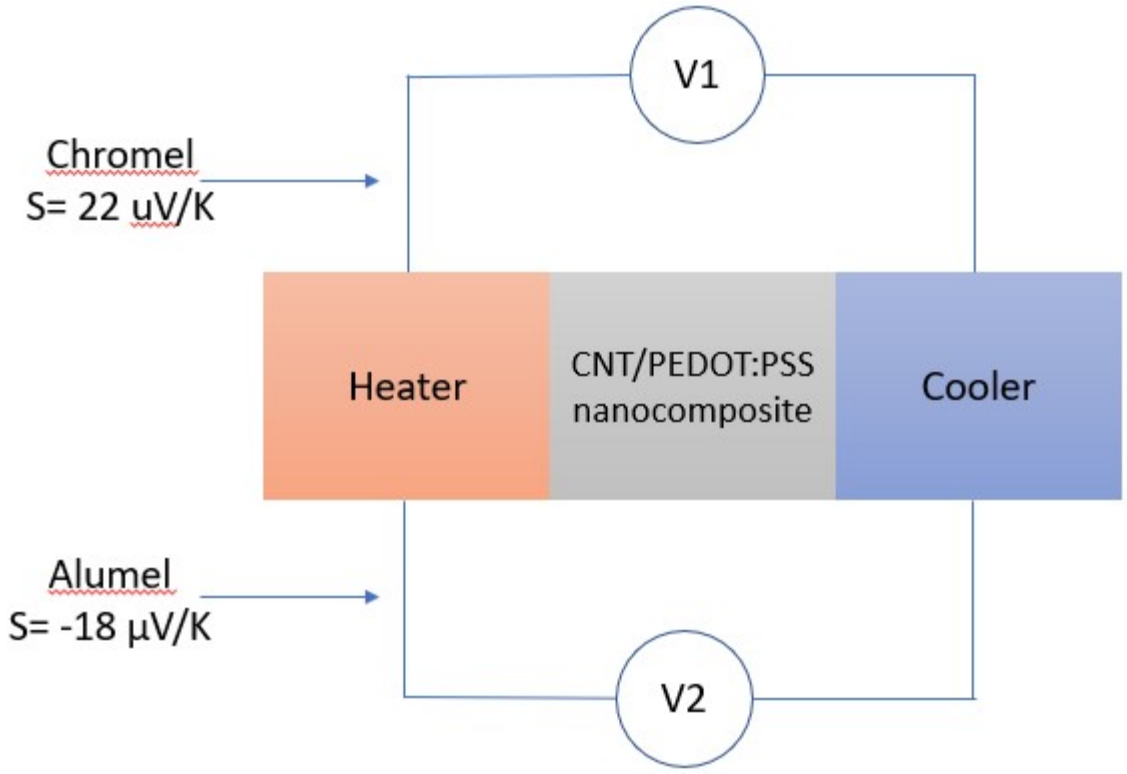


**Figure S3.** Homemade Seebeck coefficient measurement system. Detailed calculations and instructions are in Ref. [5].

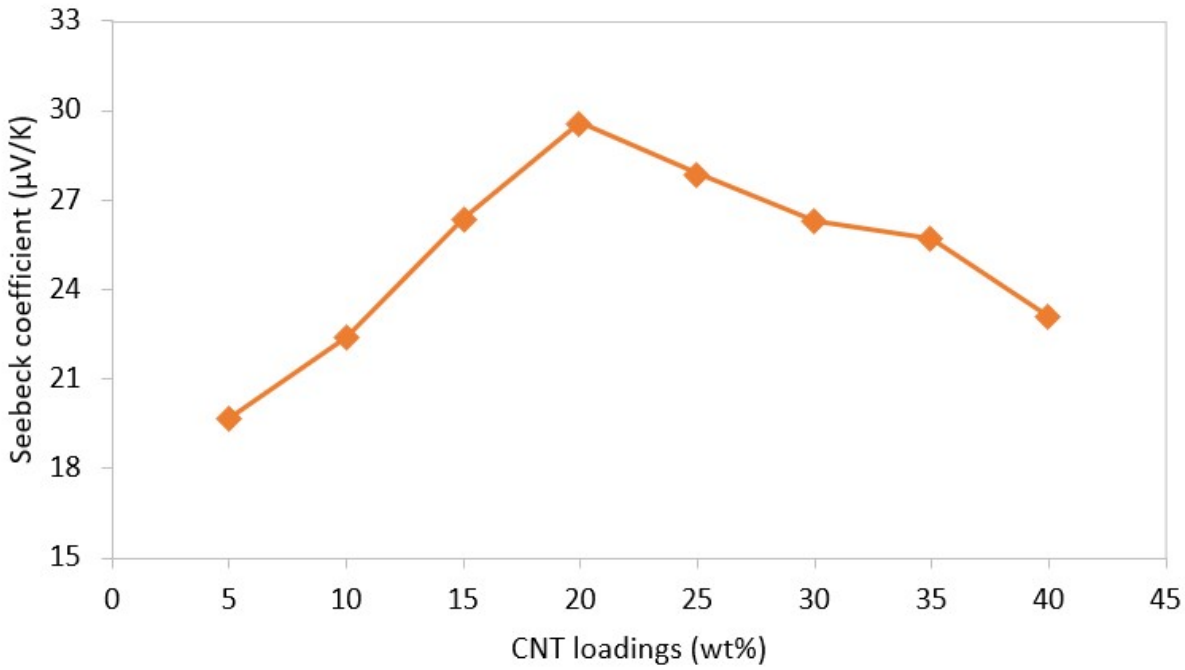


**Figure S4.** Measured Seebeck coefficient of PTE detectors of different SWCNT loadings.

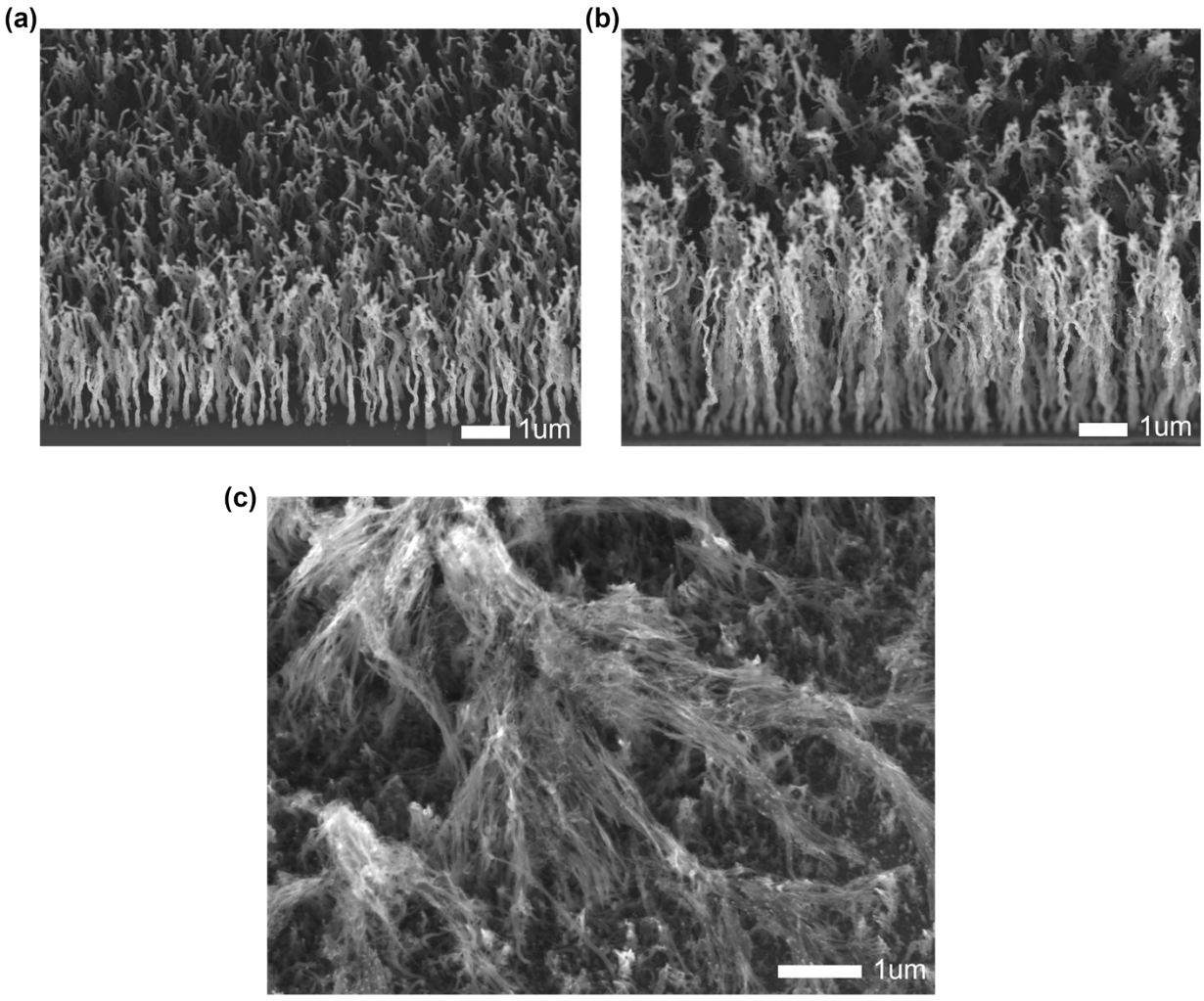


**Figure S5.** The CNT SEM with growth time of (a) 15 min, (b) 30 min, and (c) 45 min.

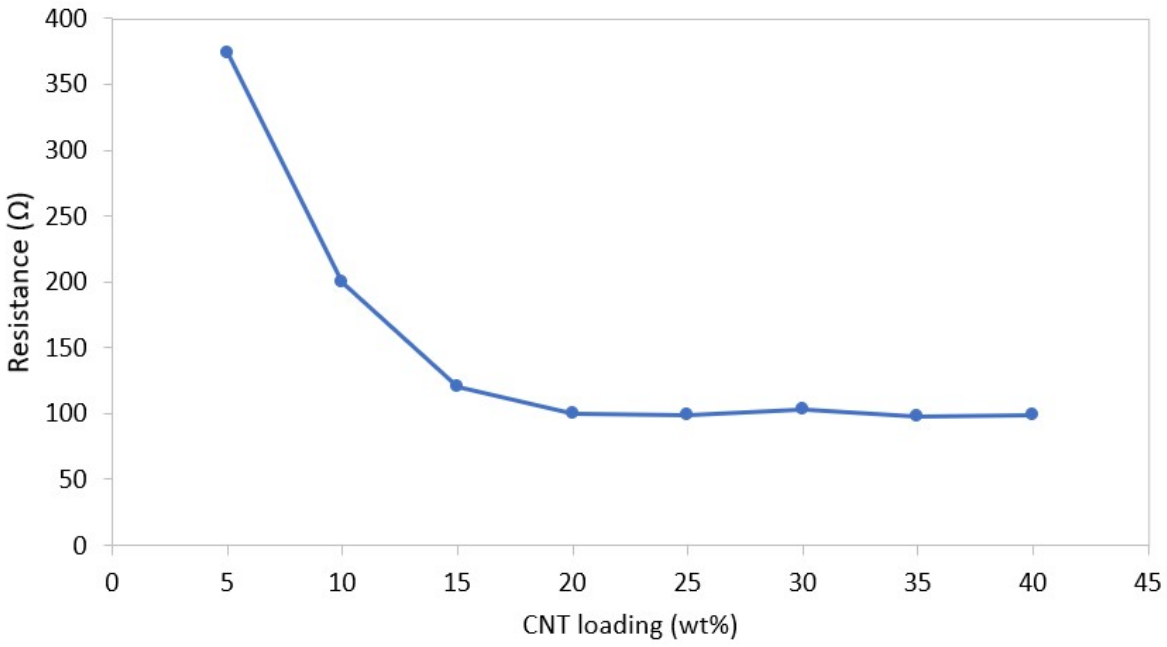


**Figure S6.** The device resistances of the SWCNT/PEDOT:PSS composite at different CNT loadings. The electrodes are 200 nm Al and 120 nm Ti.

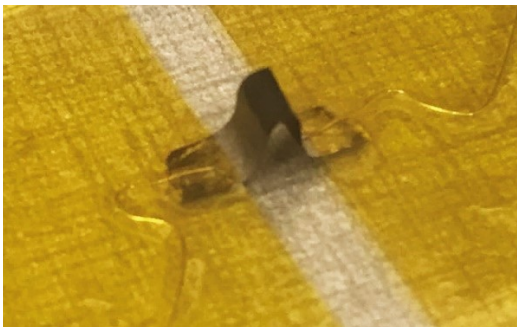

**Figure S7.** Optical imaging of the free-standing flexible PTE detector based on SWCNT/PEDOT:PSS composite.

**Photothermoelectric numerical simulation. Figure S8** shows the temperature distribution simulated by the COMSOL heat transfer module. By changing the input power, the temperature difference can be increased up to 4.0 K. The measured 29.6 μV/K Seebeck coefficient of 20 wt% SWCNT composite membrane is chosen (**Figure S4**). The measurement method can be seen in **Figure S3**. In terms of the equation of PTE voltage $U = -S \times \Delta T$, the calculated photovoltage is 10-140 μV, which is slightly higher than the experimental value. The photocurrent can be also calculated using $I = \frac{U}{R}$. With the device resistance of 100 Ω, the photocurrent value is 0.1-1.4 μA, which matches well with the actual photocurrent value. We attribute this reason to the ignored thermal diffusion between the device and the ambient environment, and the practical temperature should be lower than the simulation value.

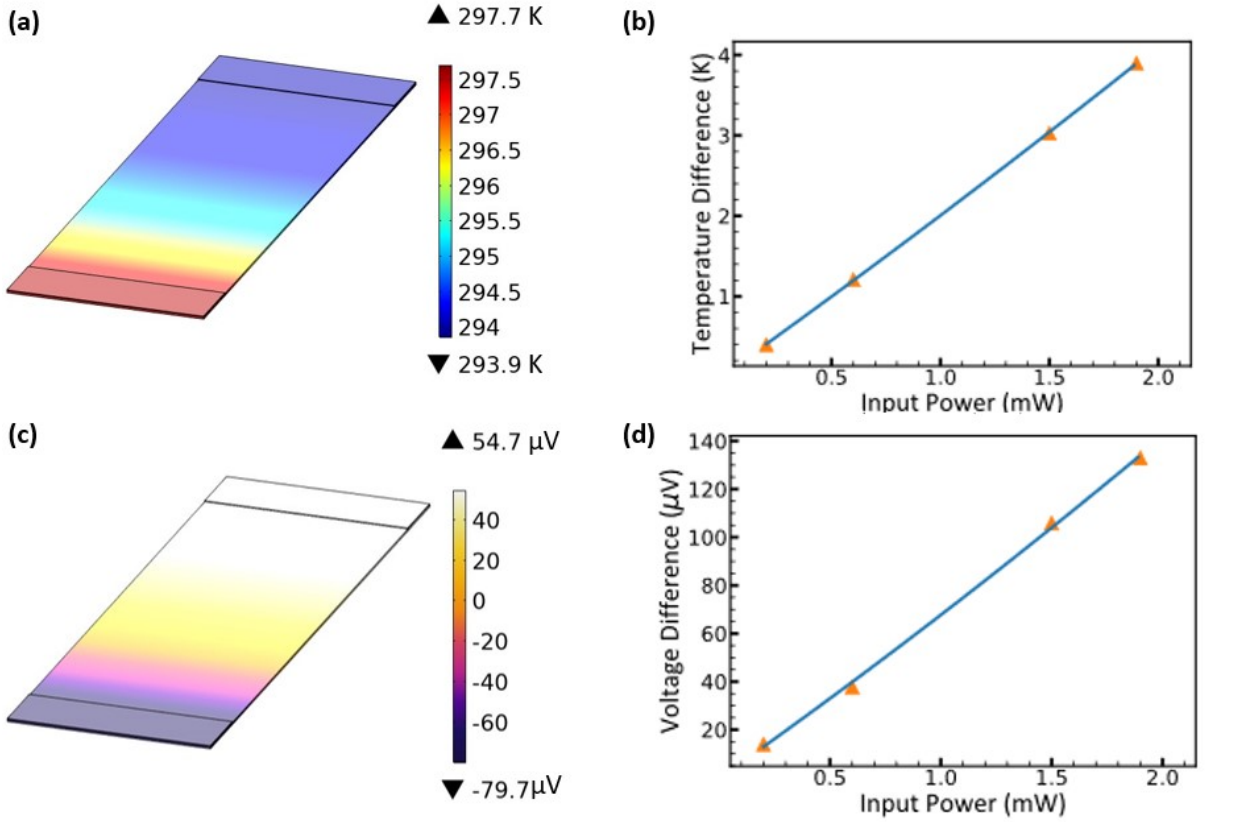


**Figure S8.** (a) Simulated voltage difference mapping of SWCNT/PEDOT:PSS composite. (b) Simulated results of voltage differences under different input power. (c) Simulated temperature difference mapping of the PTE detector under 2 mW deposited power. (d) Simulated results of temperature differences under different input power.

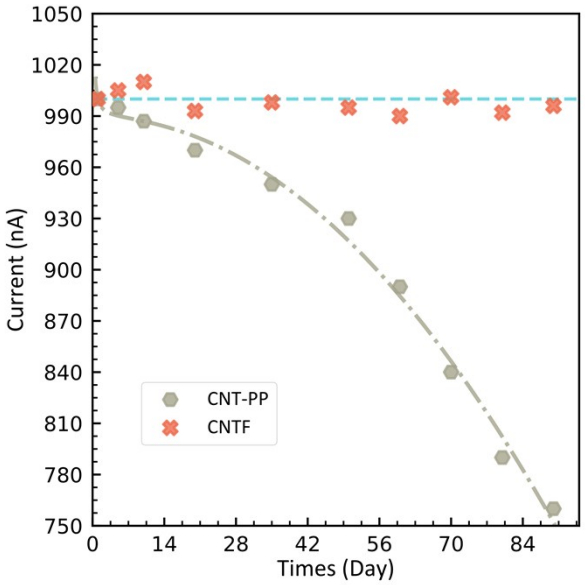


**Figure S9.** Ambient environment stability of suspended SWCNT/PEDOT:PSS composite and Si-based CNTF/PEDOT:PSS PTE detector.

**Table S1.** Comparison between this work and representative PTE detectors in MWIR/LWIR regime.

| *Active material* | *Response time* | *Wavelength (μm)* | *Responsivity* | *Detectivity (Jones)* | *Bias voltage* | *Flexibility* | *Ref* |
|---|---|---|---|---|---|---|---|
| *$EuBiSe_3$* | ~200 ms | 118.8 | 0.69 V/W | $1.17\times10^8$ | 0 | No | [6] |
| *$CH_3NH_3PbI_3$* | 126 ns | 10.6 | 483 mA/W | $2.6\times10^7$ | 1 V for responsivity<br>0.01 V for detectivity | No | [7] |
| *RGO-Si nanowire heterojunction* | 10 s | 10.6 | 1.65 mA/W (923.15 K) | - | 1V | No | [8] |
| *$SrTiO_3$* | 1.5 s | 10.6 | 1.2 V/W | - | 0 | No | [9] |
| *SWCNT/PEDOT:PSS composite* | MWIR/LWIR | 2.47-5.06 | 0.16 V/W | $1.9\times10^7$ | 0 | Yes | This work |
| *CNTF/PEDOT:PSS Composite* | MWIR/LWIR | 2.47-5.06 | 0.12 | $1.7\times10^7$ | 0 | No | |

**References**


(1) Zhou, J.; Lubineau, G. Improving Electrical Conductivity in Polycarbonate Nanocomposites Using Highly Conductive PEDOT/PSS Coated MWCNTs. *ACS Appl. Mater. Interfaces* **2013**, *5*, 6189–6200.

(2) Savva, A.; Wustoni, S.; Inal, S. Ionic-to-Electronic Coupling Efficiency in PEDOT:PSS Films Operated in Aqueous Electrolytes. *J. Mater. Chem. C* **2018**, *6*, 12023–12030.

(3) Mannayil, J.; Methattel Raman, S.; Sankaran, J.; Raman, R.; Madambi Kunjukutan Ezhuthachan, J. Solution Processable PEDOT:PSS/Multiwalled Carbon Nanotube Composite Films for Flexible Electrode Applications. *Phys. Status Solidi Appl. Mater. Sci.* **2018**, *215*, 1–10.

(4) Zhang, M.; Yeow, J. T. W. A Flexible, Scalable, and Self-Powered Mid-Infrared Detector Based on Transparent PEDOT: PSS/Graphene Composite. *Carbon N. Y.* **2020**, *156*, 339–345.

(5) Suzuki, D.; Ochiai, Y.; Nakagawa, Y.; Kuwahara, Y.; Saito, T.; Kawano, Y. Fermi-Level-Controlled Semiconducting-Separated Carbon Nanotube Films for Flexible Terahertz Imagers. *ACS Appl. Nano Mater.* **2018**, *1*, 2469–2475.

(6) Wang, Y.; Niu, Y.; Chen, M.; Wen, J.; Wu, W.; Jin, Y.; Wu, D.; Zhao, Z. Ultrabroadband, Sensitive, and Fast Photodetection with Needle-Like $EuBiSe_3$ Single Crystal. *ACS Photonics* **2019**, *6*, 895–903.

(7) Li, Y.; Zhang, Y.; Li, T.; Li, M.; Chen, Z.; Li, Q.; Zhao, H.; Sheng, Q.; Shi, W.; Yao, J. Ultrabroadband, Ultraviolet to Terahertz, and High Sensitivity $CH_3NH_3PbI_3$Perovskite Photodetectors. *Nano Lett.* **2020**, *20*, 5646–5654.

(8) Cao, Y.; Zhu, J.; Xu, J.; He, J.; Sun, J.-L.; Wang, Y.; Zhao, Z. Ultra-Broadband Photodetector for the Visible to Terahertz Range by Self-Assembling Reduced Graphene Oxide-Silicon Nanowire Array Heterojunctions. *Small* **2014**, *10*, 2345–2351.

(9) Lu, X.; Jiang, P.; Bao, X. Phonon-Enhanced Photothermoelectric Effect in $SrTiO_3$ Ultra-Broadband Photodetector. *Nat. Commun.* **2019**, *10*, 1–7.